

Quantum Mechanics Under a Momentum Space Artificial Magnetic Field

Hannah M. Price, Tomoki Ozawa and Iacopo Carusotto

INO-CNR BEC Center and Dipartimento di Fisica, Università di Trento, I-38123 Povo, Italy

The Berry curvature is a geometrical property of an energy band which acts as a momentum space magnetic field in the effective Hamiltonian describing single-particle quantum dynamics. We show how this perspective may be exploited to study systems directly relevant to ultracold gases and photonics. Given the exchanged roles of momentum and position, we demonstrate that the global topology of momentum space is crucially important. We propose a simple experiment to study the Harper-Hofstadter Hamiltonian with a harmonic trap that will illustrate the advantages of this approach and that will also constitute the first realisation of magnetism on a torus.

The Hamiltonian of a charged particle in an electromagnetic field is a familiar and fundamental result in quantum mechanics[1]. In this Hamiltonian,

$$\mathcal{H} = \frac{(\mathbf{p} - e\mathbf{A}(\mathbf{r}))^2}{2M} + e\Phi(\mathbf{r}), \quad (1)$$

the roles of momentum and position are inherently asymmetric; the magnetic vector potential, $\mathbf{A}(\mathbf{r})$, is a function of position which re-defines the relationship between the canonical, \mathbf{p} , and physical, $\mathbf{p} - e\mathbf{A}(\mathbf{r})$, momenta. The vector potential $\mathbf{A}(\mathbf{r})$ is also responsible for the geometric Aharonov-Bohm phase, which depends on the real-space trajectory of a particle.

The magnetic Hamiltonian has an important *momentum space* counterpart,

$$\tilde{\mathcal{H}} = E(\mathbf{p}) + W(\mathbf{r} + \mathcal{A}(\mathbf{p})), \quad (2)$$

that underlies many intriguing phenomena in solid state physics such as the anomalous[2–4] and spin Hall effects[5–7] as well as peculiar features of graphene[8, 9] and bulk Rashba semiconductors[10]. In this formalism, $E(\mathbf{p})$ is the energy dispersion of the band under consideration, while $\mathcal{A}(\mathbf{p})$ is the geometrical Berry connection of the band (defined below) [2, 6, 11]. The Berry connection acts as a momentum space vector potential, re-defining the relationship between the canonical, \mathbf{r} , and physical, $\mathbf{r} + \mathcal{A}(\mathbf{p})$, position operators appearing in the external potential term $W(\mathbf{r} + \mathcal{A}(\mathbf{p}))$. This replacement has important physical consequences that have been studied primarily, so far, at the semiclassical level [2, 3, 5–7, 12, 13]. As in the Aharonov-Bohm effect, a particle moving in momentum space under the influence of an external force gains a geometrical Berry phase due to the connection $\mathcal{A}(\mathbf{p})$. The curvature, $\Omega(\mathbf{p}) = \nabla_{\mathbf{p}} \times \mathcal{A}(\mathbf{p})$, also naturally defines a momentum space magnetic field[6, 11, 14, 15].

Local geometrical properties of energy bands can be related to global topological invariants. For example, the simplest topological invariant of a two-dimensional crystal, the so-called Chern number \mathcal{C} , is the integral of the Berry curvature over the first Brillouin zone. In the analogy with magnetism, the Chern number is the momentum space counterpart of the number of magnetic monopoles[16] surrounded by the surface of a torus. This

important invariant underlies the quantisation of conductance in the quantum Hall effect[17], while other topological invariants can be defined to classify topological insulators[18, 19].

In the last few years, geometrically non-trivial bands have been created in ultracold gases[20–23] and photonic systems[24–27]. Non-zero $\Omega(\mathbf{p})$ can have consequences for the collective modes of an ultracold atomic gas[28, 29] and for the semiclassical dynamics of a wave packet[30–35], while the hallmarks of nontrivial topological bands have been observed in topologically protected photonic edge states[24–26].

In this Letter, we discuss how the momentum space magnetic Hamiltonian (2) can be exploited as a fully quantum theory to understand the quantum mechanics of single particles in energy bands with non-trivial geometrical and topological properties, in the presence of additional external potentials. To illustrate this most clearly, we focus on the example of a two-dimensional system where the energy and the Berry curvature of the lowest energy band are nearly flat over the first Brillouin zone (BZ). In the presence of an external harmonic potential, the equispaced eigenstates are then the momentum space counterpart of Landau levels in a constant magnetic field. Remarkably, these eigenstates have novel features directly stemming from the global toroidal topology of the BZ. The recent experimental realisations of the Harper-Hofstadter model in ultracold gases[22, 23], photonic systems[26] and solid-state superlattices[36] suggest a prompt experimental implementation of our approach. This would open up new avenues to experimentally investigate quantum mechanics and quantum magnetism on a topologically non-trivial manifold such as a torus[37, 38].

The Effective Quantum Hamiltonian.— We start by presenting a short derivation of the momentum space magnetic Hamiltonian (2) in simple and modern terms for systems of current experimental interest. Our derivation builds on ideas over the last sixty years[2, 11, 39] and is applicable to the generic single-particle Hamiltonian, $\mathcal{H} = \mathcal{H}_0 + W(\mathbf{r})$ whose first term, \mathcal{H}_0 , is either translationally invariant or periodic in real space. For example, \mathcal{H}_0 could refer to an electron in a crystal, an atom with spin-orbit coupling, an ultracold atomic gas in an optical

lattice or light in either a photonic crystal or a lattice of coupled resonators or waveguides. The second part of the Hamiltonian, $W(\mathbf{r})$, is a weaker and slower-varying additional potential. This could be, for instance, an external static electric field for an electron, a harmonic trap or optical superlattice potential for atoms, or a slow modulation of the background refractive index and/or of the cavity size in optical systems.

The eigenfunctions of \mathcal{H}_0 can be written as $|\chi_{n,\mathbf{p}}(\mathbf{r})\rangle = \frac{e^{i\mathbf{p}\cdot\mathbf{r}}}{\sqrt{V}}|n\mathbf{p}\rangle$, where $|n\mathbf{p}\rangle$ is the energy eigenstate for band index n and momentum \mathbf{p} , and V is a normalisation factor. If \mathcal{H}_0 is periodic, the eigenstate is the periodic Bloch function, $u_{n,\mathbf{p}}(\mathbf{r})$, and the momentum is the crystal momentum defined in the BZ (we take $\hbar = 1$ throughout). The normalisation, V , is the number of lattice sites, N . If instead \mathcal{H}_0 is translationally invariant, the eigenstate $|n\mathbf{p}\rangle$ is a position-independent wave function and V is the volume of the system. For simplicity, we focus on systems in 2D, although the extension to three dimensions is straightforward.

The energy bands have a band structure, $E_n(\mathbf{p})$, and geometrical properties encoded in the Berry connection, $\mathcal{A}_n(\mathbf{p})$, and Berry curvature, $\Omega_n(\mathbf{p})$ [11, 40]:

$$\mathcal{A}_n(\mathbf{p}) \equiv i\langle n\mathbf{p}|\frac{\partial}{\partial\mathbf{p}}|n\mathbf{p}\rangle, \quad (3)$$

$$\Omega_n(\mathbf{p}) \equiv \nabla_{\mathbf{p}} \times \mathcal{A}_n(\mathbf{p}) \cdot \hat{\mathbf{z}}. \quad (4)$$

The additional potential, $W(\mathbf{r})$, mixes different eigenstates, $|n\mathbf{p}\rangle$. We expand the eigenstates of the full Hamiltonian, \mathcal{H} , as $|\Psi\rangle = \sum_n \sum_{\mathbf{p}} \psi_n(\mathbf{p})|\chi_{n,\mathbf{p}}\rangle$, where $\psi_n(\mathbf{p})$ are expansion coefficients. For a periodic \mathcal{H}_0 , this sum is taken over the first Brillouin zone, otherwise, the sum runs over all momenta. We substitute into the Schrödinger equation, $i\frac{\partial}{\partial t}|\Psi\rangle = \mathcal{H}|\Psi\rangle$, and apply $\langle\chi_{n',\mathbf{p}}|$, to obtain:

$$i\frac{\partial}{\partial t}\psi_n(\mathbf{p}) = E_n(\mathbf{p})\psi_n(\mathbf{p}) + \sum_n \sum_{\mathbf{p}} \langle\chi_{n',\mathbf{p}}|W(\mathbf{r})|\chi_{n,\mathbf{p}}\rangle\psi_n(\mathbf{p}). \quad (5)$$

To proceed, we expand $W(\mathbf{r})$ as a power series in \mathbf{r} , and repeatedly insert the completeness relation: $1 = \sum_n \sum_{\mathbf{p}} |\chi_{n,\mathbf{p}}\rangle\langle\chi_{n,\mathbf{p}}|$. (We demonstrate this explicitly in the Supplementary Information for a harmonic trap.) Then we can use the identity:

$$\langle\chi_{n',\mathbf{p}}|\mathbf{r}|\chi_{n,\mathbf{p}}\rangle = \delta_{\mathbf{p},\mathbf{p}'} \left(\delta_{n,n'} i\nabla_{\mathbf{p}} + i\langle n'\mathbf{p}'|\frac{\partial}{\partial\mathbf{p}}|n\mathbf{p}\rangle \right),$$

which we have generalised from a previously known result[2, 39](Supplementary Information). We assume that the additional potential is sufficiently weak that it does not significantly mix energy bands and that the contribution from only one band n is non-negligible. A quantitative condition for this approximation will be discussed in the following. The effective quantum Hamiltonian in

the single-band approximation then has the form (2) with the suitable $E_n(\mathbf{p})$ and $\mathcal{A}_n(\mathbf{p})$. Of course, this Hamiltonian may also be generalised to systems with degeneracies such as graphene and topological insulators[18, 19]; in this case, the effective momentum space magnetic field has a non-Abelian gauge structure[6, 41].

Connections with Magnetism.— The duality between momentum space magnetism and real space magnetism is transparently demonstrated by comparing the effective Hamiltonian (2) to the textbook magnetic Hamiltonian of a charged particle (1). The energy bandstructure, $E_n(\mathbf{p})$, acts like the external scalar potential $e\Phi(\mathbf{r})$, while the external potential $W(i\nabla_{\mathbf{p}} + \mathcal{A}_n(\mathbf{p}))$ corresponds to the “kinetic energy”, $\frac{1}{2M}(\mathbf{p} - e\mathbf{A}(\mathbf{r}))^2$ [42]. For a harmonic trapping potential, $W(\mathbf{r}) = \frac{1}{2}\kappa\mathbf{r}^2$, the effective momentum space Hamiltonian (2) has the form:

$$\tilde{\mathcal{H}} = E_n(\mathbf{p}) + \frac{\kappa(i\nabla_{\mathbf{p}} + \mathcal{A}_n(\mathbf{p}))^2}{2}, \quad (6)$$

where the inverse trapping strength, κ^{-1} plays the role of the mass of the particle, M . In the following we shall focus on this case, but other forms of the energy-momentum relationship in the real space magnetic Hamiltonian could be obtained by applying different types of external potential, $W(\mathbf{r})$.

The Topology of the Momentum Space.— The global properties of the Berry connection and curvature have been deeply investigated as they are related to topological invariants, that underlie, for example, the most striking features of the quantum Hall effect [17]. However, much less attention has been devoted to the impact of the global topology of momentum space on the particle wave function which must be single-valued[1]. This condition is of course irrelevant when the momentum \mathbf{p} can take arbitrarily large values, e.g. for particles with 2D Rashba spin-orbit coupling in a Zeeman field [29], but has very interesting consequences in spatially periodic systems where the momentum is defined over the BZ, which has the topology of a torus.

The Harper-Hofstadter Model with a Harmonic Trap.— As a concrete example of the power of our approach, we investigate the eigenstates of the Harper-Hofstadter Hamiltonian[43] with an external harmonic trap; such an experiment would be a natural extension of recent advances[22, 23, 26, 36]. In the Harper-Hofstadter model, a particle hops on a 2D lattice in a perpendicular (real or artificial) magnetic field, $\mathbf{B} = B\hat{\mathbf{z}}$. Choosing the magnetic vector potential in the Landau gauge, $\mathbf{A}(\mathbf{r}) = Bx\hat{\mathbf{y}}$, the tight-binding Hamiltonian with a harmonic trap is:

$$\mathcal{H} = \mathcal{H}_0 + \frac{1}{2}\kappa a^2 \sum_{m,n} (m^2 + n^2) \hat{a}_{m,n}^\dagger \hat{a}_{m,n},$$

$$\mathcal{H}_0 = -J \sum_{m,n} \left(\hat{a}_{m+1,n}^\dagger \hat{a}_{m,n} + e^{i\phi} \hat{a}_{m,n+1}^\dagger \hat{a}_{m,n} \right) + \text{h.c.} \quad (7)$$

where \mathcal{H}_0 is the Harper-Hofstadter Hamiltonian, J is the hopping amplitude, a is the lattice spacing and the $\hat{a}_{m,n}^\dagger$

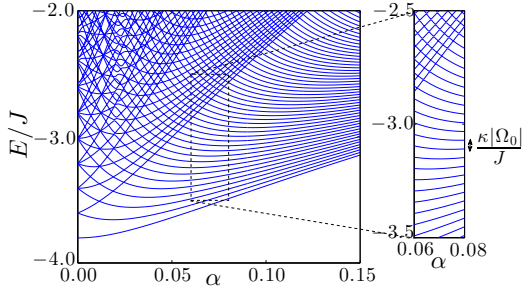


FIG. 1. The low energy spectrum obtained from a numerical diagonalisation of Eq. 7, for a harmonic trapping strength of $\kappa a^2/J = 0.02$ and a lattice with $N = 21 \times 21$ sites. The inset is an enlargement of the spectrum, highlighting the equal spacing of toroidal Landau levels.

($\hat{a}_{m,n}$) operators create (annihilate) a particle at lattice site (m, n) . The hopping along \hat{y} is modified by a complex phase $\phi = 2\pi\alpha ma$, where α is the number of magnetic flux quanta per plaquette of the lattice.

Without a harmonic trap, the eigenstates are those of the Harper-Hofstadter Hamiltonian, \mathcal{H}_0 , and the behaviour is governed by the value of α . For rational values of $\alpha = p/q$, the tight-binding band splits into q magnetic sub-bands. The energy spectrum of this Hamiltonian is the well-known Hofstadter butterfly[43]. The magnetic vector potential, $\mathbf{A}(\mathbf{r})$, is not periodic, and the usual translation operators do not commute with \mathcal{H}_0 [31]. Bloch's theorem can be applied only when we define new magnetic translation operators which do commute. For these to also commute amongst themselves, we define a larger magnetic unit cell of q plaquettes, containing an integer number of magnetic flux quanta. Then the Bloch states are *magnetic* Bloch states and the crystal momentum is defined within the *magnetic* Brillouin zone (MBZ): $-\pi/a < p_y \leq \pi/a$ and $-\pi/qa < p_x \leq \pi/qa$ (for a magnetic unit cell of q plaquettes along \hat{x}) [31].

In the presence of the harmonic trap, the external potential splits the Harper-Hofstadter bands into a complicated structure first noted in Ref. 44. Numerically calculated spectra are shown in Fig. 1 for $\kappa a^2/J = 0.02$ on a lattice of 21 by 21 sites. For each value of the magnetic flux, α , the energy levels have been obtained by numerically diagonalizing the full Hamiltonian (7). In the following, we shall show how the momentum space magnetic Hamiltonian (2) provides a clear and intuitive physical understanding of the eigenstate structure.

We focus on the regime $\alpha = 1/q \ll 1$ so that we can make two simplifications. Firstly, with decreasing $\alpha = 1/q$, the bands flatten compared to the hopping energy J . If the bandwidth is much smaller than κa^2 , we can assume $E_n(\mathbf{p}) \simeq E_n$. The effect of the band structure is then only to shift the overall energy. Secondly, when $\alpha = 1/q$ and q is odd, the Chern number of each band, except the middle band, is -1. For $\alpha \ll 1$, the Berry curvature of

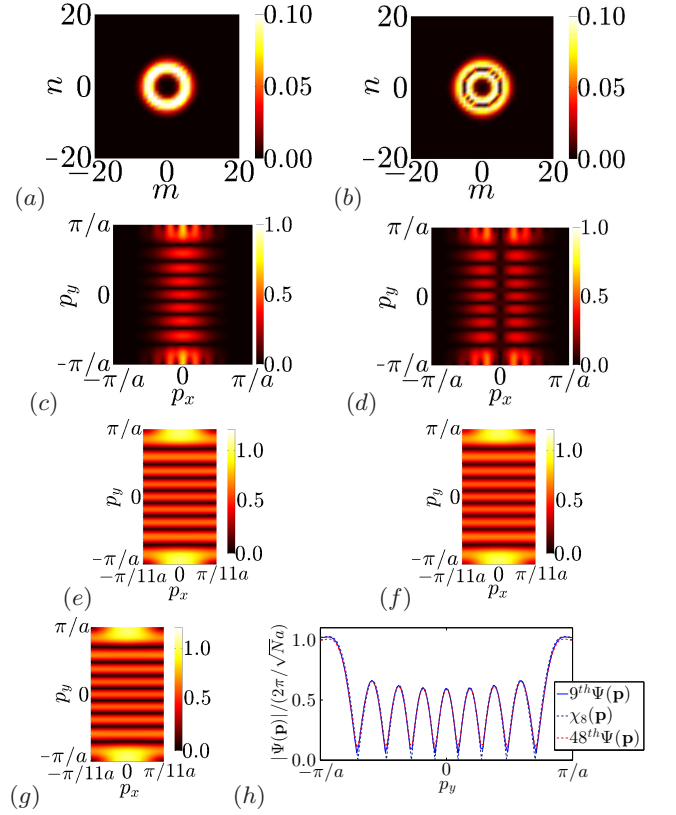


FIG. 2. (a)&(b) The wave function, $|\psi(\mathbf{r})|$, in units of a^{-1} . (c)&(d) The absolute value of the Fourier transform of $\psi(\mathbf{r})$, in units of $(2\pi/\sqrt{Na})^{-1}$, in the full Brillouin zone (see Supplementary Information for details). (e)&(f) The wave function, $|\psi(\mathbf{p})|$, in the magnetic Brillouin zone, in units of $(2\pi/\sqrt{Na})^{-1}$. The left (right) column is the 9th (48th) lowest eigenstate of Eq. (7) for $\alpha = 1/11$, $\kappa a^2/J = 0.02$ and a lattice of $N = 133 \times 133$ sites. (g) The theoretical $\beta = 8$ toroidal Landau level with $|\Omega| = a^2/(2\pi\alpha)$ (Eq. 9). (h) A quantitative comparison of a cut along $p_x = 0$ taken from (e), (f) & (g).

these bands is increasingly uniform, $\Omega_n(\mathbf{p}) \simeq \Omega_n$ [33, 45, 46]. The uniform value of the Berry curvature, $|\Omega_n| = a^2/(2\pi\alpha)$, is found by noting that the Chern number: $\mathcal{C}_n = \frac{1}{2\pi}\Omega_n A_{\text{BZ}} = -1$, where $A_{\text{BZ}} = (2\pi)^2/qa^2$ is the area of the MBZ[29]. Therefore for $\alpha = 1/q \ll 1$, the single-band effective Hamiltonian (2) describes a particle in a uniform magnetic field in momentum space, with an additional overall energy shift.

The eigenstates of a particle in a real space uniform magnetic field are the infinitely degenerate Landau levels[1]. Introducing periodic boundary conditions restricts the particle to the surface of a torus. As has long been studied theoretically, toroidal Landau levels are superpositions of the infinitely degenerate Landau levels such that the boundary conditions are satisfied[37, 38]. From the duality between momentum space magnetism and real space magnetism, we can deduce the properties of toroidal Landau levels in the magnetic Brillouin zone. The energy is unaffected by topology and is given by the

well-known Landau level spectrum:

$$\mathcal{E}_{n,\beta} = E_n + \left[\beta + \frac{1}{2} \right] \kappa |\Omega_n|, \quad (8)$$

where E_n is the energy of the original Harper-Hofstadter band, $\beta = 0, 1, 2, \dots$ is the Landau level quantum number and $\kappa |\Omega_n|$ is the analogue of the cyclotron frequency, $\omega_c = e|B|/M$. The degeneracy of toroidal Landau levels is finite and equal to the quantised number of magnetic flux quanta piercing the torus[37]. Counting the degeneracy of such states may therefore provide another experimental tool to directly measure the Chern number of non-degenerate energy bands.

This analytical prediction is confirmed by the numerical spectrum shown in the inset of Fig. 1; in the lower part of the spectrum, one sees that the lowest Harper-Hofstadter $n = 0$ band is split into a ladder of equispaced states. The energy spacing of these states is in excellent agreement with the momentum space analog (8) of the cyclotron frequency, where $|\Omega_0| = a^2/(2\pi\alpha)$. The result was also noted in Ref. 44 but its origin was not discussed there. These states are non-degenerate reflecting the Chern number of the lowest band.

Looking at higher energies in the inset of Fig. 1, one notes that a second ladder of equispaced states cuts diagonally across the first ladder. These states can be identified as toroidal Landau levels in the second lowest Harper-Hofstadter band; the similar spacing is a consequence of both bands having the same Chern number, while the overall upwards shift is due to the energy difference, $(E_1 - E_0)$, between the two underlying bands.

As one can see in the main panel of Fig. 1, this simple structure of Landau levels of course holds only over a finite range of α . At large α , the \mathbf{p} dependence of $\Omega_n(\mathbf{p})$ and of $E_n(\mathbf{p})$ is no longer negligible. At small α , the Harper-Hofstadter bands are too close for the single-band approximation to hold, and one recovers the energy spacing of approximately $\kappa a^2/J$ that is expected for a 2D simple harmonic oscillator on a tight-binding lattice[44]. Quantitatively, the single band approximation requires that $\kappa a^2 \ll (E_n - E_{n'})$. This is easily fulfilled for our choice of parameters: the splitting of the two lowest bands in the absence of the trap, for example, is $(E_1 - E_0) \simeq J$ for $\alpha = 1/11$, so the effective Hamiltonian applies to each band separately, without inter-band coupling. This is apparent in the figure as the levels originating from different bands freely cross without significant coupling.

Note also that, even though our analytical calculation is restricted to $\alpha = 1/q$, the numerical calculation shows that the spectrum continuously depends on α . The analytical explanation of this feature in the general $p > 1$ case requires application of the magnetic model to (almost) degenerate bands with non-Abelian Berry connection, which will be the subject of a future publication.

To further verify our interpretation, we can also compare the form of the numerical eigenstates with those of theoretical Landau levels on a torus[38]. In the magnetic Brillouin zone, when $|\mathcal{C}_n| = 1$, the states are:

$$\begin{aligned} \chi_\beta(\mathbf{p}) = \mathcal{N}_\beta^{l_{\Omega_n}} \sum_{j=-\infty}^{\infty} e^{ip_y j a} e^{-(p_x - j a l_{\Omega_n}^2)^2 / 2 l_{\Omega_n}^2} \\ \times H_\beta(p_x / l_{\Omega_n} - j a l_{\Omega_n}), \end{aligned} \quad (9)$$

where H_β are Hermite polynomials and $\mathcal{N}_\beta^{l_{\Omega_n}}$ is a normalisation constant (Supplementary Information). The characteristic momentum scale is $l_{\Omega_n} = \sqrt{1/|\Omega_n|}$, the analogue of the “magnetic length”, $l_B = \sqrt{1/e|B|}$. The excellent agreement between toroidal Landau levels and the numerical eigenstates is shown in Fig. 2, for the 9th and 48th numerical states, which correspond to the $\beta = 8$ toroidal Landau level in the lowest and second Harper-Hofstadter bands respectively. As expected from the analytical model, the momentum space wave function in the MBZ, $\psi(\mathbf{p})$, is mostly determined by the Landau level quantum number β only and is therefore almost identical in the different bands (as demonstrated in panels (e-h)). On the other hand, the real space wave functions, shown in panels (a,b), are markedly different as they depend on the band index, n , through the Bloch wave functions $u_{n,\mathbf{p}}(\mathbf{r})$.

We also note that, like a real space magnetic vector potential, the momentum space Berry connection is gauge-dependent, while the Berry curvature is not. In writing the analytical wave function (9), we chose the Landau gauge for the Berry connection, $\mathcal{A}_n(\mathbf{p}) = |\Omega_n| p_x \hat{\mathbf{p}}_y$, however, we only compare quantities that are independent of the choice of momentum space gauge with numerics.

Finally, we have checked that the Landau levels observed are remarkably robust to variation in the parameters, making our proposal well suited to experimental investigation. According to our numerics, the basic features of the lowest energy toroidal Landau levels survive for magnetic flux up to $\alpha = 1/5$ and for $\kappa a^2/J \simeq 0.5$. This gives a large parameter regime over which the properties of the effective magnetic Hamiltonian may be investigated. Importantly, these results are also very insensitive to lattice size, due to strong localisation of the low energy eigenstates in real space (Fig. 2). This is because toroidal Landau levels are delocalised in momentum space, varying over a large characteristic momentum-scale, l_{Ω_n} . Therefore, experiments can be performed for very small lattices, which is a key technical advantage.

Experimentally, a harmonic trap can be straightforwardly added to an ultracold atomic gas by means of additional laser beams and/or magnetic fields. The momentum space structure of the eigenstates can be probed directly in time-of-flight measurements of the momentum distribution, when both the lattice and the artificial magnetic field responsible for the complex hopping terms

in (7) are suddenly switched off. While the real space wave function, shown in Fig. 2 (a,b), is independent of the gauge choice of the Harper-Hofstadter Hamiltonian, the momentum space wave function is not. However, this experimental procedure automatically selects for \mathcal{H}_0 the gauge for which the canonical and physical momenta coincide in the final time-of-flight expansion stage [22, 23, 47]. Similar features occur in photonic systems; a harmonic potential can be created in the cavity arrays of Refs. 26 and 27 by letting the cavity size vary in space, while the real (momentum) space wave function can be extracted from the near-field (far-field) emitted light [27, 48].

In summary, we have discussed how future experiments may use external potentials and geometrical energy bands to design novel magnetic Hamiltonians in momentum space. As a first step, we have shown how a particle in a uniform magnetic field confined to a torus may be realised experimentally for the first time using either ultra-cold atomic gases or photonic systems. There also remain many interesting open questions, such as the possibility of quantum mechanics on manifolds with more complex topologies than that of a torus, and of momentum space electrodynamics when the band structure is made to slowly vary in time. Finally, as contact interactions in real space translate into strongly nonlocal interactions in momentum space, we can anticipate that inclusion of interactions in suitable conditions will open up the way towards new, exotic quantum states of matter.

We are grateful to N. R. Cooper for helpful comments and to P. Ghiggini for mathematical support. This work was partially funded by ERC through the QGBE grant and by the Autonomous Province of Trento, Call “Grandi Progetti 2012,” project “On silicon chip quantum optics for quantum computing and secure communications - SiQuro”.

-
- [1] L. D. Landau and L. M. Lifshitz, *Quantum Mechanics, Third Edition: Volume 3*, 3rd ed. (Butterworth-Heinemann, Oxford, 1958).
 - [2] E. N. Adams and E. I. Blount, J. Phys. Chem. Solids **10**, 286 (1959).
 - [3] N. Nagaosa, J. Sinova, S. Onoda, A. H. MacDonald, and N. P. Ong, Rev. Mod. Phys. **82**, 1539 (2010).
 - [4] F. D. M. Haldane, Phys. Rev. Lett. **93**, 206602 (2004).
 - [5] S. Murakami, N. Nagaosa, and S.-C. Zhang, Science **301**, 1348 (2003).
 - [6] K. Y. Bliokh and Y. P. Bliokh, Ann. Phys. **319**, 13 (2005).
 - [7] T. Fujita, M. B. A. Jalil, S. G. Tan, and S. Murakami, J. Appl. Phys. **110**, 121301 (2011).
 - [8] K. S. Novoselov *et al.*, Nature **438**, 197 (2005).
 - [9] Y. B. Zhang, Y. W. Tan, H. L. Stormer, and P. Kim, Nature **438**, 201 (2005).
 - [10] H. Murakawa *et al.*, Science **342**, 1490 (2013).
 - [11] M. V. Berry, Proc. R. Soc. London, Ser. A **392**, 45 (1984).
 - [12] K. Y. Bliokh, Europhys. Lett. **72**, 7 (2005).
 - [13] P. Gosselin, F. Ménas, A. Bérard, and H. Mohrbach, Europhys. Lett. **76**, 651 (2006).
 - [14] T. T. Wu and C. N. Yang, Phys. Rev. D **12**, 3845 (1975).
 - [15] N. Cooper and R. Moessner, Phys. Rev. Lett. **109**, 215302 (2012).
 - [16] Z. Fang *et al.*, Science **302**, 92 (2003).
 - [17] D. J. Thouless, M. Kohmoto, M. P. Nightingale, and M. den Nijs, Phys. Rev. Lett. **49**, 405 (1982).
 - [18] M. Z. Hasan and C. L. Kane, Rev. Mod. Phys. **82**, 3045 (2010).
 - [19] X.-L. Qi and S.-C. Zhang, Rev. Mod. Phys. **83**, 1057 (2011).
 - [20] L. Tarruell, D. Greif, T. Uehlinger, G. Jotzu, and T. Esslinger, Nature **483**, 302 (2012).
 - [21] J. Struck *et al.*, Nature Phys. **9**, 738 (2013).
 - [22] M. Aidelsburger *et al.*, Phys. Rev. Lett. **111**, 185301 (2013).
 - [23] H. Miyake, G. A. Siviloglou, C. J. Kennedy, W. C. Burton, and W. Ketterle, Phys. Rev. Lett. **111**, 185302 (2013).
 - [24] Z. Wang, Y. Chong, J. D. Joannopoulos, and M. Soljačić, Nature **461**, 772 (2009).
 - [25] M. C. Rechtsman *et al.*, Nature **496**, 196 (2013).
 - [26] M. Hafezi, S. Mittal, J. Fan, A. Migdall, and J. M. Taylor, Nature Photon. **7**, 1001 (2013).
 - [27] T. Jacqmin *et al.*, Phys. Rev. Lett. **112**, 116402 (2014).
 - [28] E. van der Bijl and R. A. Duine, Phys. Rev. Lett. **107**, 195302 (2011).
 - [29] H. M. Price and N. R. Cooper, Phys. Rev. Lett. **111**, 220407 (2013).
 - [30] A. M. Dudarev, R. B. Diener, I. Carusotto, and Q. Niu, Phys. Rev. Lett. **92**, 153005 (2004).
 - [31] M.-C. Chang and Q. Niu, Phys. Rev. Lett. **75**, 1348 (1995).
 - [32] H. M. Price and N. R. Cooper, Phys. Rev. A **85**, 033620 (2012).
 - [33] M. Cominotti and I. Carusotto, Europhys. Lett. **103**, 10001 (2013).
 - [34] A. Dauphin and N. Goldman, Phys. Rev. Lett. **111**, 135302 (2013).
 - [35] T. Ozawa and I. Carusotto, Phys. Rev. Lett. **112**, 133902 (2014).
 - [36] C. R. Dean *et al.*, Nature **497**, 598 (2013).
 - [37] J. K. Jain, *Composite Fermions* (Cambridge University Press, Cambridge, 2007).
 - [38] M. H. Al-Hashimi and U.-J. Wiese, Ann. Phys. **324**, 343 (2009).
 - [39] R. Karplus and J. M. Luttinger, Phys. Rev. **95**, 1154 (1954).
 - [40] D. Xiao, M.-C. Chang, and Q. Niu, Rev. Mod. Phys. **82**, 1959 (2010).
 - [41] F. Wilczek and A. Zee, Phys. Rev. Lett. **52**, 2111 (1984).
 - [42] This viewpoint has previously been discussed for the specific case of a particle with 2D Rashba spin-orbit coupling in a harmonic trap in Ref. 49.
 - [43] D. R. Hofstadter, Phys. Rev. B **14**, 2239 (1976).
 - [44] A. R. Kolovsky, F. Grusdt, and M. Fleischhauer, Phys. Rev. A **89**, 033607 (2014).
 - [45] J. Zak, Phys. Rev. Lett. **62**, 2747 (1989).
 - [46] F. Harper, S. H. Simon, and R. Roy, arXiv preprint

- arXiv:1404.5303 (2014).
- [47] Y.-J. Lin, R. L. Compton, K. Jiménez-García, W. D. Phillips, J. V. Porto, and I. B. Spielman, *Nature Phys.* **7**, 531 (2011).
- [48] I. Carusotto and C. Ciuti, *Rev. Mod. Phys.* **85**, 299 (2013).
- [49] Y. Li, X. Zhou, and C. Wu, *Phys. Rev. B* **85**, 125122 (2012).

**SUPPLEMENTARY INFORMATION:
THE BERRY CURVATURE AS A MAGNETIC FIELD IN MOMENTUM SPACE**

Appendix A: Derivation of The Effective Hamiltonian for an External Harmonic Trap

Here we explicitly derive the effective Hamiltonian for an external harmonic trap, $W(\mathbf{r}) = \frac{1}{2}\kappa\mathbf{r}^2$. We begin from the Schrödinger equation, expanded in terms of the eigenstates of \mathcal{H}_0 :

$$i\frac{\partial}{\partial t}\psi_n(\mathbf{p}) = E_n(\mathbf{p})\psi_n(\mathbf{p}) + \sum_n \sum_{\mathbf{p}} \frac{\kappa}{2} \langle \chi_{n',\mathbf{p}'} | \mathbf{r}^2 | \chi_{n,\mathbf{p}} \rangle \psi_n(\mathbf{p}). \quad (\text{A1})$$

In the last line, we insert the completeness relation of Bloch states, $1 = \sum_n \sum_{\mathbf{p}} |\chi_{n,\mathbf{p}}\rangle \langle \chi_{n,\mathbf{p}}|$:

$$i\frac{\partial}{\partial t}\psi_n(\mathbf{p}) = E_n(\mathbf{p})\psi_n(\mathbf{p}) + \frac{\kappa}{2} \sum_{n,n''} \sum_{\mathbf{p},\mathbf{p}''} \langle \chi_{n',\mathbf{p}'} | \mathbf{r} | \chi_{n'',\mathbf{p}''} \rangle \langle \chi_{n'',\mathbf{p}''} | \mathbf{r} | \chi_{n,\mathbf{p}} \rangle \psi_n(\mathbf{p}) \quad (\text{A2})$$

Now that the Schrödinger equation is in this form, we can apply an identity to replace terms of the type: $\langle \chi_{n',\mathbf{p}'} | \mathbf{r} | \chi_{n,\mathbf{p}} \rangle$. This identity is a generalised version of a result originally due to Karplus and Luttinger[1]. The derivation is as follows:

$$\begin{aligned} \langle \chi_{n',\mathbf{p}'} | \mathbf{r} | \chi_{n,\mathbf{p}} \rangle &= \int d^2\mathbf{r} w_{n',\mathbf{p}'}^*(\mathbf{r}) e^{-i\mathbf{p}'\cdot\mathbf{r}} e^{i\mathbf{p}\cdot\mathbf{r}} w_{n,\mathbf{p}}(\mathbf{r}) \\ &= -i \int d^2\mathbf{r} w_{n',\mathbf{p}'}^*(\mathbf{r}) e^{-i\mathbf{p}'\cdot\mathbf{r}} (\nabla_{\mathbf{p}} e^{i\mathbf{p}\cdot\mathbf{r}}) w_{n,\mathbf{p}}(\mathbf{r}) \\ &= -i \nabla_{\mathbf{p}} \left[\int d^2\mathbf{r} e^{-i(\mathbf{p}'-\mathbf{p})\cdot\mathbf{r}} w_{n',\mathbf{p}'}^*(\mathbf{r}) w_{n,\mathbf{p}}(\mathbf{r}) \right] + i \int d^2\mathbf{r} e^{-i(\mathbf{p}'-\mathbf{p})\cdot\mathbf{r}} w_{n',\mathbf{p}'}^*(\mathbf{r}) \nabla_{\mathbf{p}} w_{n,\mathbf{p}}(\mathbf{r}), \end{aligned} \quad (\text{A3})$$

where $w_{n,\mathbf{p}}(\mathbf{r}) = \langle \mathbf{r} | n\mathbf{p} \rangle$. If \mathcal{H}_0 is periodic, the momentum is the crystal momentum and $w_{n,\mathbf{p}}(\mathbf{r}) = u_{n,\mathbf{p}}(\mathbf{r})$. As the Bloch functions are periodic, the last integral will vanish[1] unless $\mathbf{p} = \mathbf{p}'$. Otherwise, if \mathcal{H}_0 is not periodic, then $w_{n,\mathbf{p}}(\mathbf{r}) = w_{n,\mathbf{p}}$ is independent of position. Then the last integral will also vanish unless $\mathbf{p} = \mathbf{p}'$. Using the orthonormality of the eigenfunctions, and integrating the derivative of the delta function by parts, we obtain the identity:

$$\langle \chi_{n',\mathbf{p}'} | \mathbf{r} | \chi_{n,\mathbf{p}} \rangle = \delta_{\mathbf{p},\mathbf{p}'} \left(\delta_{n,n'} i \nabla_{\mathbf{p}'} + i \langle n' | \mathbf{p}' | \frac{\partial}{\partial \mathbf{p}} | n \mathbf{p} \rangle \right). \quad (\text{A4})$$

We can recognise the last term as the generalised non-Abelian Berry connection[2]: $\mathcal{A}_{n',n}(\mathbf{p}) = i \langle n' | \mathbf{p} | \frac{\partial}{\partial \mathbf{p}} | n \mathbf{p} \rangle$. Substituting the identity into the Schrödinger equation, we find:

$$i\frac{\partial}{\partial t}\psi_n(\mathbf{p}) = E_n(\mathbf{p})\psi_n(\mathbf{p}) + \frac{\kappa}{2} \sum_{n,n''} (\delta_{n',n''} i \nabla_{\mathbf{p}} + \mathcal{A}_{n',n''}(\mathbf{p})) \cdot (\delta_{n'',n} i \nabla_{\mathbf{p}} + \mathcal{A}_{n'',n}(\mathbf{p})) \psi_n(\mathbf{p}). \quad (\text{A5})$$

If we assume that the external potential does not significantly mix energy bands, we can make a single band approximation. The Schrödinger equation then reduces to:

$$i\frac{\partial}{\partial t}\psi_n(\mathbf{p}) = \left[E_n(\mathbf{p}) + \frac{\kappa}{2} (i \nabla_{\mathbf{p}} + \mathcal{A}_n(\mathbf{p}))^2 \right] \psi_n(\mathbf{p}). \quad (\text{A6})$$

We note that the Schrödinger equation could equally have been restricted to a sub-space of degenerate or nearly degenerate bands that are well-separated in energy from other bands. Then the sums in Eq. A5 only run over this sub-space of bands. The corresponding Berry curvature has a non-Abelian gauge structure[3, 4]. Physically, an energy band Hamiltonian containing the non-Abelian Berry connection, $\mathcal{A}_{n',n}(\mathbf{p})$, may describe quantum spin Hall models, graphene or topological insulators[5, 6] in additional potentials.

Appendix B: Extracting the Eigenstates in the Magnetic Brillouin Zone from the Numerics of the Harper-Hofstadter Model with a Harmonic Trap

Here we show how the eigenstates of the Harper-Hofstadter Hamiltonian with a harmonic trap can be obtained numerically in the magnetic Brillouin zone. We diagonalise the Hamiltonian to find the numerical energy eigenstates

in real space:

$$|\Psi\rangle = \sum_{m,n} \psi(m,n) a_{m,n}^\dagger |0\rangle, \quad (\text{B1})$$

where $\psi(m,n)$ are the eigenfunction coefficients for each lattice site. (The eigenstates are normalised to a lattice of area Na^2 .) To observe toroidal Landau levels, this wave-function must be transformed into the MBZ. We first Fourier transform the real space wave function, to find:

$$|\Psi\rangle = \sum_{\tilde{p}_x, \tilde{p}_y} \psi(\tilde{p}_x, \tilde{p}_y) a_{\tilde{p}_x, \tilde{p}_y}^\dagger |0\rangle, \quad (\text{B2})$$

where $\tilde{\mathbf{p}} = (\tilde{p}_x, \tilde{p}_y)$ is the crystal momentum in the *full* Brillouin zone: $-\pi/a < \tilde{\mathbf{p}} \leq \pi/a$. (For simplicity of presentation in Fig. 2 in the main text, we denote both the momentum in the *full* Brillouin zone and the magnetic Brillouin zone by \mathbf{p}).

We note that the magnetic Brillouin zone is defined from the Harper-Hofstadter Hamiltonian without a harmonic trap[7, 8]. For clarity, we demonstrate this by taking the Fourier transform of the lattice creation and annihilation operators:

$$\begin{aligned} \hat{a}_{m,n} &= \sum_{\tilde{p}_x, \tilde{p}_y} e^{i\tilde{p}_x m a + i\tilde{p}_y n a} \hat{a}_{\tilde{p}_x, \tilde{p}_y}, \\ \hat{a}_{m,n}^\dagger &= \sum_{\tilde{p}_x, \tilde{p}_y} e^{-i\tilde{p}_x m a - i\tilde{p}_y n a} \hat{a}_{\tilde{p}_x, \tilde{p}_y}^\dagger, \end{aligned} \quad (\text{B3})$$

and substituting them into \mathcal{H}_0 . After simplifying the algebra, the Harper-Hofstadter Hamiltonian in the full Brillouin zone becomes[9]:

$$\mathcal{H}_0 = \sum_{\tilde{p}_x, \tilde{p}_y} [-2J \cos(\tilde{p}_x a) \hat{a}_{\tilde{p}_x, \tilde{p}_y}^\dagger \hat{a}_{\tilde{p}_x, \tilde{p}_y} - J(e^{-i\tilde{p}_y a} \hat{a}_{\tilde{p}_x + 2\pi\alpha/a, \tilde{p}_y}^\dagger \hat{a}_{\tilde{p}_x, \tilde{p}_y} + e^{i\tilde{p}_y a} \hat{a}_{\tilde{p}_x - 2\pi\alpha/a, \tilde{p}_y}^\dagger \hat{a}_{\tilde{p}_x, \tilde{p}_y})]. \quad (\text{B4})$$

This is not diagonal in the full Brillouin zone, as \tilde{p}_x is mixed with $\tilde{p}_x + 2\pi\alpha/a$ and $\tilde{p}_x - 2\pi\alpha/a$. However, the Hamiltonian can be made diagonal, by defining a new variable: $p_x = \tilde{p}_x + j2\pi\alpha/a$, where j is an integer. For $\alpha = 1/q$, $\mathbf{G} = 2\pi\alpha/a\hat{p}_x$ is a magnetic reciprocal lattice vector for the unit cell discussed in the text, and \mathbf{p} is the magnetic crystal momentum. Note that the choice of the new variable, \mathbf{p} , followed naturally from the magnetic gauge of \mathcal{H}_0 . We have deliberately picked the magnetic unit cell for which: $\mathbf{p} = \tilde{\mathbf{p}} + j\mathbf{G}$. (For other choices of magnetic unit cell, this relation would not generally take this simple form.) We can then write:

$$|\chi_{n,\mathbf{p}}\rangle = \sum_{\tilde{\mathbf{p}}} U_{n,\mathbf{p}}(\tilde{\mathbf{p}}) \hat{a}_{\tilde{\mathbf{p}}}^\dagger |0\rangle, \quad (\text{B5})$$

where $U_{n,\mathbf{p}}(\tilde{\mathbf{p}})$ is a unitary matrix that transforms eigenstates between the full and magnetic Brillouin zone. This matrix only has non-zero values for $\tilde{\mathbf{p}} = \mathbf{p} - j\mathbf{G}$. Taking the inverse of Eq. B5 and applying it to Eq. B2, we have:

$$\begin{aligned} |\Psi\rangle &= \sum_{n,\mathbf{p},\tilde{\mathbf{p}}} U_{n,\mathbf{p}}^*(\tilde{\mathbf{p}}) \psi(\tilde{\mathbf{p}}) |\chi_{n,\mathbf{p}}\rangle \\ &= \sum_{n,\mathbf{p}} \psi_n(\mathbf{p}) |\chi_{n,\mathbf{p}}\rangle, \end{aligned} \quad (\text{B6})$$

where $\psi_n(\mathbf{p})$ are the wave function coefficients in the magnetic Brillouin zone. Then it follows that:

$$\sum_n |\psi_n(\mathbf{p})|^2 = \sum_j |\psi(\tilde{\mathbf{p}} = \mathbf{p} - j\mathbf{G})|^2. \quad (\text{B7})$$

If we make the single band approximation, and assume that $\psi_n(\mathbf{p})$ is only non-negligible in one band, we obtain $|\psi_n(\mathbf{p})|^2 = \sum_j |\psi(\tilde{\mathbf{p}} = \mathbf{p} - j\mathbf{G})|^2$. This relationship is used to calculate the numerical wave function in the magnetic Brillouin zone in the main text & below in Fig. C1.

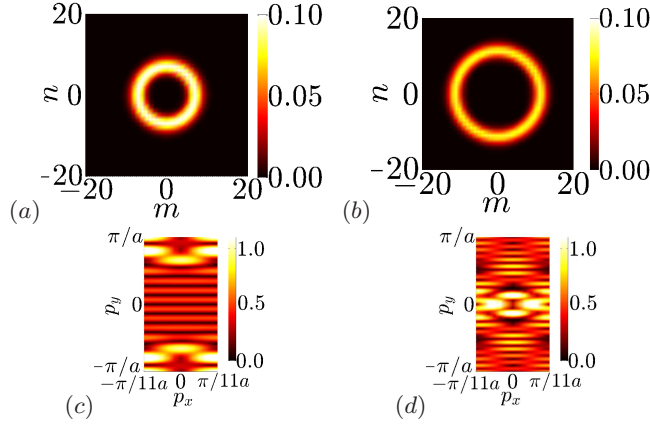


FIG. C1. (a)&(b) The wave function, $|\psi(\mathbf{r})|$, in units of a^{-1} . The left (right) figure is the 16th (49th) lowest eigenstate of the Harper-Hofstadter Hamiltonian with a harmonic trap for $\alpha = 1/11$, $\kappa a^2/J = 0.02$ and $N = (133)^2$. (c)&(d) The wave-function, $|\psi(\mathbf{p})|$, in the magnetic Brillouin zone, in units of $(2\pi/\sqrt{N}a)^{-1}$. The left (right) figure is in excellent agreement with the $\beta = 15$ ($\beta = 39$) toroidal Landau level in the lowest band (Eq. C1).

Appendix C: Further Details for Toroidal Landau Levels

Here we give further details and examples of toroidal Landau levels. As stated in the main text, for $|\mathcal{C}_n| = 1$, these have the form:

$$\chi_\beta(\mathbf{p}) = \mathcal{N}_\beta^{l_{\Omega_n}} \sum_{j=-\infty}^{\infty} e^{ip_y j a} e^{-(p_x - j a l_{\Omega_n}^2)^2 / 2l_{\Omega_n}^2} H_\beta(p_x / l_{\Omega_n} - j a l_{\Omega_n}) \quad (\text{C1})$$

translated from the theoretical Landau levels of a particle on a real space torus[10]. We note that the form of these levels depends on the Chern number and the dimensions of the magnetic Brillouin zone. The wave function obeys periodic boundary conditions and the “solenoid fluxes” are zero. The normalisation constant is:

$$\mathcal{N}_\beta^{l_{\Omega_n}} = \left(\frac{\sqrt{2/q}}{(2^\beta \beta! \times 2\pi l_{\Omega_n}^2)} \right)^{1/2}. \quad (\text{C2})$$

Further examples of toroidal Landau levels are shown in Figure C1. These are again in excellent agreement with theoretical toroidal Landau levels (C1). The importance of the topology of the space is apparent from a comparison of these states with the usual plane wave basis of Landau levels:

$$\chi_\beta(\mathbf{p}) \propto e^{ip_y y} e^{-(p_x - y l_{\Omega_n}^2)^2 / 2l_{\Omega_n}^2} H_\beta(p_x / l_{\Omega_n} - y l_{\Omega_n}), \quad (\text{C3})$$

where \mathbf{p} varies continuously over all momenta and is not constrained to the Brillouin zone. (The Berry connection is again chosen in the Landau gauge specified in the main text). The wave functions of this basis of Landau levels are characterised by a plane wave along p_y , and β nodes along p_x . In the same gauge, the toroidal Landau levels have a markedly different structure (Fig. C1 c & d). The toroidal Landau levels vary along both momenta directions, with the majority of nodes along p_y .

-
- [1] R. Karplus and J. M. Luttinger, Phys. Rev. **95**, 1154 (1954).
 - [2] D. Xiao, M.-C. Chang, and Q. Niu, Rev. Mod. Phys. **82**, 1959 (2010).
 - [3] F. Wilczek and A. Zee, Phys. Rev. Lett. **52**, 2111 (1984).
 - [4] K. Y. Bliokh and Y. P. Bliokh, Ann. Phys. **319**, 13 (2005).
 - [5] M. Z. Hasan and C. L. Kane, Rev. Mod. Phys. **82**, 3045 (2010).
 - [6] X.-L. Qi and S.-C. Zhang, Rev. Mod. Phys. **83**, 1057 (2011).
 - [7] M. Kohmoto, Ann. Phys. **160**, 343 (1985).
 - [8] M.-C. Chang and Q. Niu, Phys. Rev. Lett. **75**, 1348 (1995).
 - [9] B. Bernevig and T. Hughes, *Topological Insulators and Topological Superconductors* (Princeton University Press, 2013).
 - [10] M. H. Al-Hashimi and U.-J. Wiese, Ann. Phys. **324**, 343 (2009).